ACS APPLIED MATERIALS & INTERFACES

www.acsami.org

Research Article

A Hydrogel-Integrated Culture Device to Interrogate T Cell Activation with Physicochemical Cues

Matthew H. W. Chin, Michael D. A. Norman, Eileen Gentleman, Marc-Olivier Coppens, and Richard M. Day*

Cite This: *ACS Appl. Mater. Interfaces* 2020, 12, 47355–47367

Read Online

ACCESS | Metrics & More | Article Recommendations | Supporting Information

ABSTRACT: The recent rise of adoptive T cell therapy (ATCT) as a promising cancer immunotherapy has triggered increased interest in therapeutic T cell bioprocessing. T cell activation is a critical processing step and is known to be modulated by physical parameters, such as substrate stiffness. Nevertheless, relatively little is known about how biophysical factors regulate immune cells, such as T cells. Understanding how T cell activation is modulated by physical and biochemical cues may offer novel methods to control cell behavior for therapeutic cell processing. Inspired by T cell mechanosensitivity, we developed a multiwell, reusable, customizable, two-dimensional (2D) polyacrylamide (PA) hydrogel-integrated culture device to study the physicochemical stimulation of Jurkat T cells. Substrate stiffness and ligand density were tuned by concentrations of the hydrogel cross-linker and antibody in the coating solution, respectively. We cultured Jurkat T cells on 2D hydrogels of different stiffnesses that presented surface-immobilized stimulatory antibodies against CD3 and CD28 and demonstrated that Jurkat T cells stimulated by stiff hydrogels (50.6 ± 15.1 kPa) exhibited significantly higher interleukin-2 (IL-2) secretion, but lower proliferation, than those stimulated by softer hydrogels (7.1 ± 0.4 kPa). In addition, we found that increasing anti-CD3 concentration from 10 to 30 μg/mL led to a significant increase in IL-2 secretion from cells stimulated on 7.1 ± 0.4 and 9.3 ± 2.4 kPa gels. Simultaneous tuning of substrate stiffness and stimulatory ligand density showed that the two parameters synergize (two-way ANOVA interaction effect: $p < 0.001$) to enhance IL-2 secretion. Our results demonstrate the importance of physical parameters in immune cell stimulation and highlight the potential of designing future immunostimulatory biomaterials that are mechanically tailored to balance stimulatory strength and downstream proliferative capacity of therapeutic T cells.

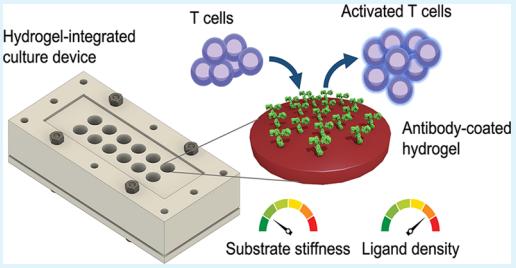

KEYWORDS: *hydrogels, mechanobiology, T cell activation, immunomodulation, substrate stiffness, immunotherapy*

1. INTRODUCTION

The ability to sense mechanical cues in the environment — mechanosensitivity — has been observed in many types of cells. This property underlies the fundamental functioning of numerous cellular processes, including cell spreading,[1] proliferation,[2] and differentiation.[3] Furthermore, mechanosensitivity is also known to play a critical role in tumorigenesis[4] and other pathological conditions. Much work in the field has focused on anchorage-dependent cells, which attach to surfaces using membrane-associated macromolecular assemblies called focal adhesions (FA).[5] However, mounting evidence suggests that cells conventionally cultured in suspension, such as lymphocytes, are also able to sense physical cues via FA-independent mechanosensory mechanisms. For instance, the T cell receptor (TCR)[6−8] and B cell receptor (BCR)[9] have both shown mechanosensing properties. In addition, recent studies have begun to unravel how mechanosensitivity enables tuning of essential immunological processes, such as T cell activation[6,7] and cytotoxic T lymphocyte (CTL)-mediated target cell killing.[10]

The emergence of adoptive T cell therapy (ATCT) has drawn attention to the study of T cell mechanobiology (Figure 1). ATCT is a form of cancer immunotherapy that augments a patient's immune system with adoptively transferred, tumor-reactive T cells.[11] Examples of ATCT include treating patients with chimeric antigen receptor (CAR) T cells,[12] TCR-transduced T cells,[13] and tumor infiltrating lymphocytes (TILs).[14]

Current ATCT manufacturing protocols often require infusion of a large number of effector T cells to generate an effective antitumor immune response.[15] In these protocols, isolated autologous T cells typically undergo *ex vivo* processing that involves stimulating activation, proliferative expansion, and differentiation. Importantly, the stimulation process is

Received: September 12, 2020
Accepted: September 18, 2020
Published: October 7, 2020

https://dx.doi.org/10.1021/acsami.0c16478
ACS Appl. Mater. Interfaces 2020, 12, 47355–47367

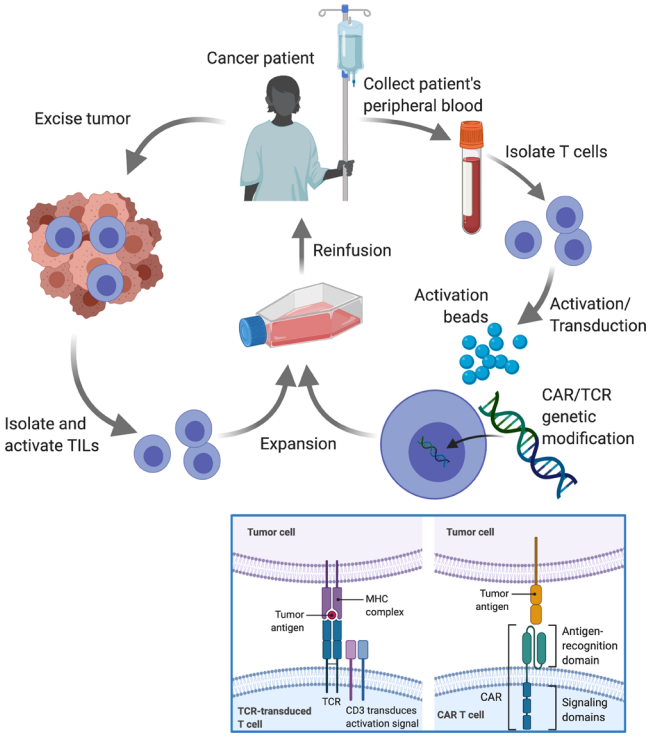

Figure 1. Simplified schematic illustrating three different types of ATCT currently in development for cancer therapy: TILs, CAR-, and TCR-transduced T cells. In general, all types require activation (typically with anti-CD3/CD28 beads) and expansion prior to reinfusion. However, for CAR-T and TCR-T cells, genetic modification is performed to equip the cells with tumor antigen-recognizing receptors. Blue box: While TCRs recognize peptides on the surface presented by the major histocompatibility complex (MHC), CARs recognize protein antigens expressed on the tumor cell surface. Since both intracellular and surface proteins can be presented as peptides in the context of MHC, transgenic TCRs have the potential to target more tumor antigens than CARs.

fundamental to acquired immunity and is normally mediated *in vivo* via the interactions between antigen-specific T cells and antigen presenting cells (APC), such as dendritic cells (DC).[16] DC present naïve antigen-specific T cells with signals required for activation − (signal 1) peptide-major histocompatibility complex (pMHC) molecules for TCR triggering, (signal 2) costimulatory molecules such as CD80 (B7−1) to ligate CD28 on the T cell, and (signal 3) mitogenic cytokines such as interleukin-2 (IL-2).[17] Signals 1 and 2 are known to be the minimum requirements to elicit full T cell activation, whereas signal 3 serves to further enhance proliferation.

In the context of ATCT, the logistical demand of harvesting and maintaining both APC and T cells has prompted the development of acellular, artificial antigen-presenting cells (aAPC) − synthetic materials that present T cell stimulatory cues.[18] To date, the most common T cell stimulation method in clinical manufacturing involves the use of commercially available anti-CD3/CD28-coated beads, such as Dynabeads (Thermo Fisher Scientific Inc.). Here, anti-CD3 provides an antigen-nonspecific signal to the TCR-CD3 complex (signal 1), and anti-CD28 delivers the costimulatory signal (signal 2).[19] These beads are often made of high-stiffness materials, such as polystyrene (3.2−3.4 GPa[20]), and, therefore, are unable to fully exploit the potential stimulatory benefits of T cell mechanosensing. The use of suboptimal biophysical cues with contemporary protocols employing anti-CD3/CD28 activation omits the opportunity to enhance aspects of the manufacturing process and risks generating suboptimal products with regard to their proliferative capacity and ability to preserve immune functionality post-infusion.[21]

The role of the TCR as a mechanosensor and the force-dependent nature of T cell activation have been widely reported.[22,23] Indeed, T cells use their TCR to sense physical cues, such as matrix stiffness, geometry, and topography.[6−8,24] Direct comparison between experimental studies and identification of key parameters is difficult due to variations in experimental design, including the choice of biomaterials, stiffness range, antibodies, conjugation methods, and T cell types. For example, using streptavidin-doped polyacrylamide (PA) hydrogels (2−200 kPa) coated with biotinylated anti-CD3/CD28, Judokusumo et al.[6] found that IL-2 production from mouse naïve $CD4^+$ T cells increased with stiffness. In contrast, O'Connor et al.[7] utilized polydimethylsiloxane (PDMS) (0.1−2 MPa) with physically adsorbed antibodies and observed an opposite trend with human naïve $CD4^+$ T cells. More recently, it has been suggested that the opposing stiffness-dependent trends might be two sides of the same coin − a biphasic response.[25] Specifically, the response becomes monotonic when ligands to T cell integrins are also present, implicating an interaction between TCR-based and integrin-based mechanoregulations. Another important parameter is the surface density of stimulatory ligands, which has been shown to regulate T cell activation.[26] All of the aforementioned studies were carried out under conditions where either stiffness or ligand density was fixed. Taken together, these observations warrant a multiparametric investigation into how T cell activation can be regulated by substrate stiffness and ligand density simultaneously using the same material.

Here, we developed a hydrogel-integrated culture device as a versatile and reusable platform to study the physicochemical modulation of T cell activation. For a proof-of-concept, anti-CD3/CD28-coated 2D PA hydrogels were explored as stiffness-tunable substrates for stimulation of Jurkat T cells. Within the device, compartmentalized hydrogel-coated microwells allowed parallel stimulation studies to be performed using a single hydrogel-coated microscope slide. Simultaneous tuning of substrate stiffness and stimulatory ligand density revealed that the two parameters synergize to enhance IL-2 secretion, a measure of T cell activation. Moreover, we showed that substrate stiffness may be exploited to balance stimulatory strength and post-stimulation cell proliferation. Taken together, the tools and approaches developed herein allow for new avenues to be explored in the design of T cell stimulatory materials and highlight the importance of biophysical cues in regulating T cell biology.

2. MATERIALS AND METHODS

2.1. Materials. 3-Aminopropyltriethoxysilane (APTES), glutaraldehyde, phosphate-buffered saline (PBS), acrylamide, *N,N′*-methylenebisacrylamide (bisacrylamide), ammonium persulfate (APS), tetramethylethylenediamine (TEMED), bovine serum albumin (BSA), Tween-20, FITC-conjugated goat anti-mouse IgG, and RPMI-1640 cell culture medium (with L-glutamine) were purchased from Sigma-Aldrich. Biotinylated mouse monoclonal antibodies − anti-human CD3ε (anti-CD3; clone: OKT3) and anti-human CD28 (anti-CD28; clone: CD28.2) − were purchased from BioLegend. Streptavidin-conjugated acrylamide, Alexa Fluor 568, fetal bovine serum (FBS), Press-to-Seal silicone sheets, and Dynabeads Human T-Activator CD3/CD28 and DynaMag-2 magnet were purchased from

https://dx.doi.org/10.1021/acsami.0c16478
ACS Appl. Mater. Interfaces 2020, 12, 47355−47367

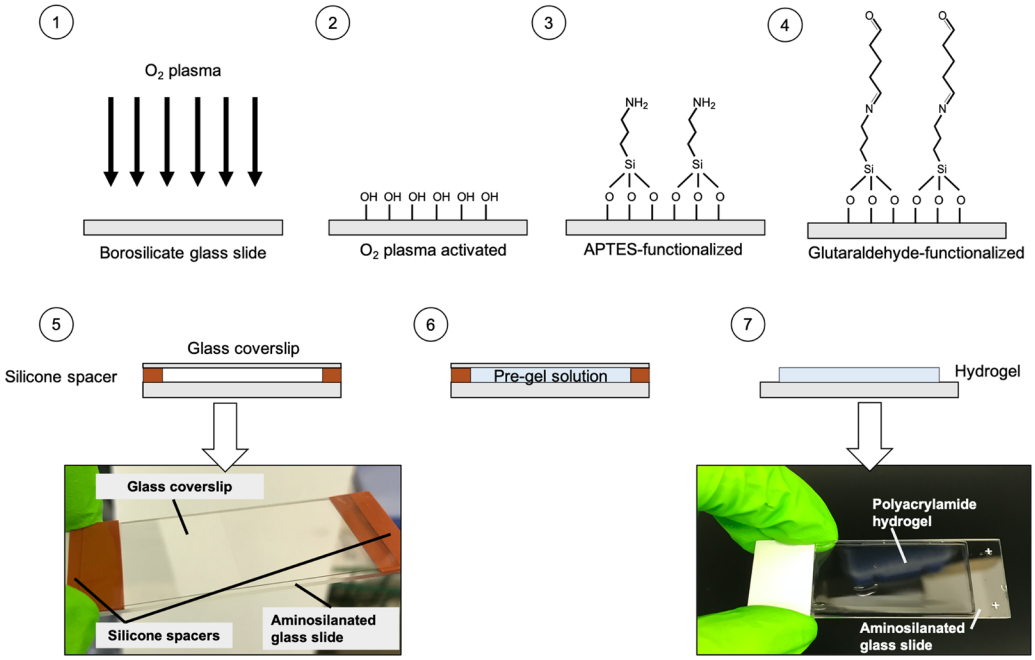

Figure 2. Schematic representation of the fabrication of PA hydrogels. (1) Borosilicate glass slides were cleaned by O_2 plasma to generate (2) silanol groups on the surface. (3) The activated glass slides were amino-silanized by APTES and (4) subsequently functionalized by glutaraldehyde. (5) A gel-casting sandwich was then set up (the arrow indicates a photograph of it) for (6) hydrogel polymerization. (7) After the polymerization, the coverslip and spacers were removed, leaving a layer of hydrogel attached to the glass slide (the arrow indicates a photograph of a hydrogel-coated slide).

Table 1. Ingredients for Polyacrylamide Hydrogel Fabrication

concentration (w/v %)			volume from stock (μL)				
acrylamide	bis-acrylamide	streptavidin-acrylamide ($\times 10^{-3}$)	40% (w/v) acrylamide	2% (w/v) bis-acrylamide	2 mg/mL streptavidin-acrylamide	1× PBS	mean stiffness in kPa (see Figure 4a)
10	0.05	1.6	250	25	8	717	7.1
10	0.1	4.0	250	50	20	680	9.3
10	0.4	70	250	200	350	200	50.6

Thermo Fisher. Human IL-2 DuoSet ELISA kits were purchased from R&D Systems. Jurkat cells were provided as a kind gift by Prof. Hans Stauss (Institute of Immunity & Transplantation, University College London). All solutions were made in PBS unless otherwise specified. The SYLGARD 184 Silicone Elastomer Kit was purchased from Dow Corning.

2.2. Preparation of PA Hydrogels. PA hydrogels were fabricated following established methods,[27] with the exception that borosilicate glass microscope slides were used as backing templates instead of glass coverslips (Figure 2). Briefly, microscope slides were first activated with oxygen plasma (0.4 mbar, 200 W, 10 mins;[28] Pico, Diener Electronic) to generate silanol (Si−OH) groups at the surface. Then, the slides were amino-silanized using APTES (0.5 mL per slide, 5 min, RT) followed by incubation with 0.5% (v/v) glutaraldehyde (30 min). Hydrogels were then created using a pre-gel solution consisting of the monomer, acrylamide, its cross-linker, bis-acrylamide, and streptavidin-conjugated acrylamide for antibody immobilization (Table 1). Hydrogels were formed via free-radical polymerization, initiated with 1:100 total volume of 10% (w/v) APS in sterile-filtered PBS and 1:1000 total volume of TEMED. The monomer-to-cross-linker ratio was varied to make gels of different stiffnesses. All pre-polymer solutions were prepared in a tissue culture cabinet.

The setup used for gel polymerization consisted of a rectangular borosilicate glass coverslip raised above an amino-silanized glass slide by 0.5 mm-thick spacers, which were cut from a Press-to-Seal silicone sheet (step 5 in Figure 2). Immediately after addition of APS and TEMED, the pre-gel solution was vortexed and pipetted into the 0.5 mm gap of the set-up. After polymerization (1 h, RT), hydrogel-coated slides were immersed in sterile PBS and washed overnight with gentle shaking at 4 °C. The next day, PBS was changed, and the hydrogels were stored at 4 °C before use. All gels were used within 2 weeks of polymerization.

2.3. Antibody Immobilization. Antibody immobilization on hydrogels was achieved by conjugating biotinylated antibodies to streptavidin-doped PA hydrogels. The procedure was performed by incubating hydrogels with antibody solution overnight at 4 °C in a sealed, humidified Petri dish. For T cell stimulation, two different antibody combinations were tested: (1) anti-CD3 only and (2) anti-CD3 and anti-CD28 (ratio 1:1). The total protein concentration in the coating solution was fixed at 10 μg/mL for all combinations, as previously described.[6,8] The antibody solution was pipetted into the gap created by spacers (1 mm-thick) between a glass coverslip and the hydrogel-coated microscope slide. This approach ensured a uniform distribution of the antibody solution over the gel surface while keeping the volume at a minimum. After overnight incubation (4 °C), the hydrogels were washed three times in PBS (5 min per wash) on an orbital shaker to remove any unbound antibodies.

2.4. Immunofluorescence Imaging. Immunofluorescence microscopy was used to confirm antibody immobilization and compare surface ligand densities. Ab-coated hydrogels were first incubated with 3% (w/v) BSA in PBST (PBS containing 0.1% (v/v) Tween-20) for 1 h at RT. Afterward, a solution of goat anti-mouse IgG (whole molecule)-FITC was added to the hydrogels at 1:200 in 3% BSA-PBST. The gels were then incubated in the dark (1 h, RT). Afterward,

https://dx.doi.org/10.1021/acsami.0c16478
ACS Appl. Mater. Interfaces 2020, 12, 47355−47367

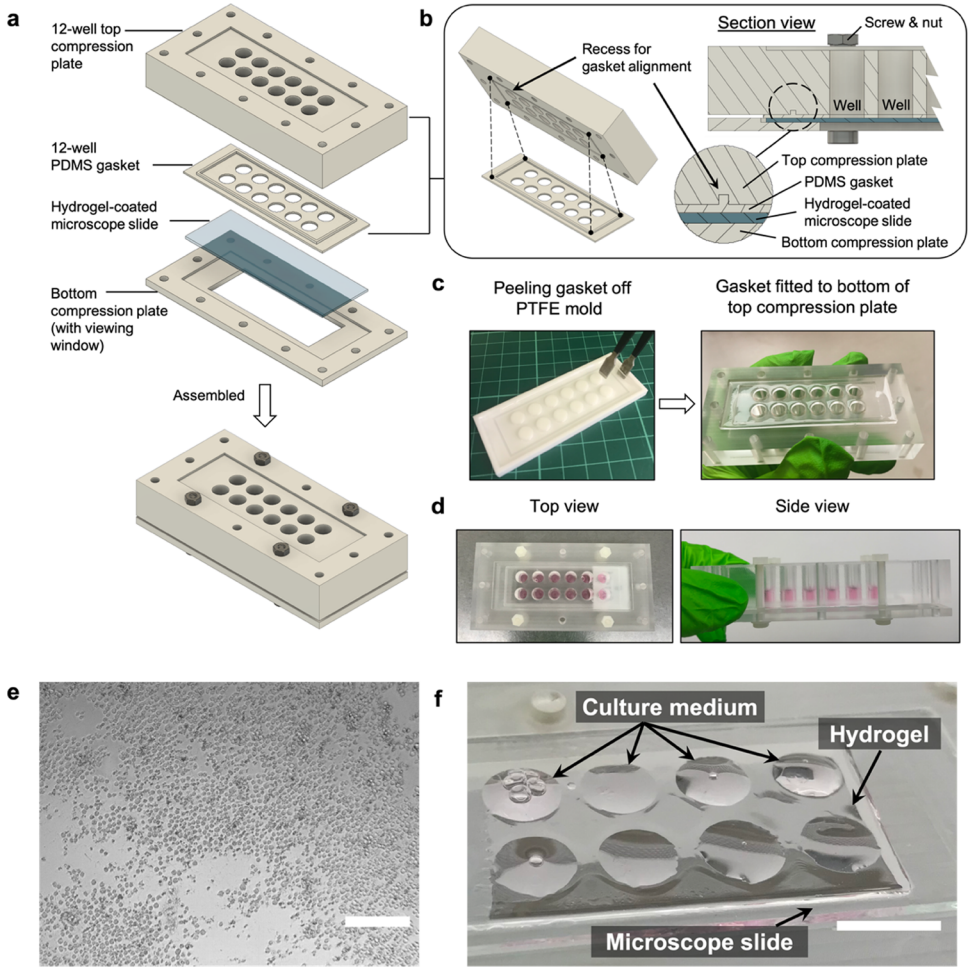

Figure 3. Hydrogel-integrated multiwell culture chamber for T cell stimulation. (a) Exploded view of the assembly. (b) The interior of the assembly with a detailed view showing how the recessed rectangular slot enabled alignment and fitting of the PDMS gasket. (c) The gasket was created using a PTFE mold and could be easily detached using tweezers (preferably with flat tips). (d) Top and side views show 200 μL of culture medium loaded in each microwell without any leakage. (e) Image of Jurkat cells inside the hydrogel-integrated culture chamber, as viewed from the bottom viewing window using an inverted phase contrast microscope. Scale bar = 100 μm. (f) A gel-coated slide removed from the assembly after aspiration of culture medium from the microwells. Residual medium formed circular droplets on the slide where the microwells were before disassembly. Scale bar = 10 mm.

the gels were washed five times in PBST (10 min per wash) before imaging.

Hydrogels were imaged using a confocal microscope (Leica TCS SPE). Image acquisition parameters were chosen for ease of visualization: format = 1024 × 1024; speed = 600 Hz; frame average = 2; gain = 912.6; laser power = 30%. Z-stack image series (25 slices of thickness 4.28 μm each) were acquired from at least three regions of interest (ROIs) per gel and three independent gels per stiffness.

Fiji (version 2.0.0-rc-65/1.51w) was used to analyze image stacks obtained from confocal microscopy. The mean fluorescence intensity (MFI) was calculated in two different ways to provide information about the spatial distribution of the fluorescence signal and its magnitude. First, z-axis profiles were generated by plotting the mean gray intensity of the ROI versus scan depth along the z-direction for each image stack. The mean gray intensities from experimental replicates and repeats were then pooled together and averaged to give an MFI for different depths. Second, the maximum intensity values along the z-axis were used to derive the MFI. Here, replicate and repeat maximum values were pooled and averaged to obtain MFI values as a single metric of surface ligand density for each experimental condition.

2.5. Hydrogel Stiffness Characterization. The Young's modulus (E) of hydrogels attached on glass slides was measured by microindentation using an atomic force microscope (Nanowizard 4 AFM, JPK Instruments). Spherical glass beads (10 μm diameter; Whitehouse Scientific) were mounted onto tipless triangular silicon nitride cantilevers (spring constant 0.12−0.24 N/m; Bruker) using UV cross-linked Loctite superglue. Prior to measurements, the deflection sensitivity of the AFM photodiode was calibrated by performing a force−distance curve on a glass slide. Cantilevers were then calibrated using the thermal noise method to confirm the spring constant.[29] At least 300 force measurements were made per stiffness, while all samples were immersed in PBS. Gels were indented 0.5−1 μm with an approach speed of 4 μm/s. E was then determined using JPK SPM software 6.1 (JPK Instruments AG) and fitted to the Hertzian model. The Poisson's ratio was assumed to be 0.5.

2.6. Cell Culture. Jurkat cells − an immortalized line of human $CD4^+$ T cells − were used as a model system due to their secretion of interleukin-2 (IL-2) upon activation.[30] Cells were cultured, according to the American Type Culture Collection (ATCC) protocol, in an RPMI-1640 medium supplemented with 2 mM L-glutamine and 10% (v/v) FBS (complete culture medium) under standard culture conditions (37 °C, 5% carbon dioxide, and 95% relative humidity). The concentration of cells was maintained between 1×10^5 and 1×10^6 viable cells/mL via addition of fresh media every 2 days, as per the ATCC protocol. Cell number and viability were quantified using Via1-Cassettes (ChemoMetec) in a NucleoCounter NC-200 automated cell counter running the Viability and Cell Count Assay.

https://dx.doi.org/10.1021/acsami.0c16478
ACS Appl. Mater. Interfaces 2020, 12, 47355−47367

2.7. Design and Fabrication of the Hydrogel-Integrated Culture Device. Hydrogel-coated microscope slides were incorporated into custom-made, reusable multiwell culture chambers (Figure 3a) for T cell stimulation experiments. The setup was formed by sandwiching a gel-coated slide between two micromilled poly(methyl methacrylate) (PMMA) compression plates. Twelve 6.4 mm through-holes in the top plate were used to compartmentalize the hydrogel into microwells. To align through-holes of the top compression plate with those of the gasket, the bottom side of the plate was micromilled along the edge to form a rectangular slot into which the protrusion feature of a PDMS gasket would fit (Figure 3b). The PDMS gasket (Figure 3c) was placed between the top plate and gel-coated slide to create a leak-free seal. It was fabricated by mixing the base elastomer and curing agent in a mass ratio of 10:1. The mixture was then cast in a micromilled polytetrafluoroethylene (PTFE) mold, degassed for 10 min, and cured at 85 °C for 2 h. The transparency of PMMA allowed contents of each well to be viewed from the side of the top compression plate (Figure 3d). The bottom plate was designed to include a rectangular window so that well contents could be inspected using inverted microscopy (Figure 3e). The entire culture chamber was held together using nylon M3 hex screws and nuts. All parts of the culture chamber and the PTFE mold were digitally designed using Autodesk's prototyping software Fusion 360. Before and after cell experiments, all parts of the culture chambers were washed with 70% ethanol and ultrapure water followed by ultraviolet (UV) sterilization in a tissue culture hood (1 h). After aspirating the culture medium, residual liquid on the gel-coated slide formed circular droplets that matched the position and dimension of the wells, which avoided cross-contamination between wells (Figure 3f).

2.8. T Cell Stimulation. A preliminary screening experiment was carried out to investigate the effect of substrate stiffness and surface ligand density on the activation of Jurkat. Streptavidin-doped PA hydrogels of different stiffnesses were coated with anti-CD3 at 10 and 30 μg/mL. Uncoated hydrogels (0 μg/mL anti-CD3) were included as a negative control. Hydrogels were equilibrated in complete culture medium for 30 min prior to cell seeding. Hydrogel surfaces were seeded with Jurkat cells at 2.7×10^5 cells/mL in 0.2 mL per well (chosen to minimize cells overlapping in the microwells and for the ease of image analysis). To avoid medium evaporation, the culture devices were placed in humidified 150 mm Petri dishes before transferring into an incubator. Cells were then incubated for 24 h under standard culture conditions before supernatants were harvested for IL-2 enzyme-linked immunosorbent assay (ELISA) analysis. A time course study was also conducted, where one well for each time point was used and supernatants were collected at 6, 24, and 48 h of stimulation.

The performance of Ab-coated hydrogels was compared with that of Dynabeads in terms of IL-2 secretion and post-stimulation proliferation. As Dynabeads were coated with both anti-CD3 and anti-CD28, the formulation of Ab-coating solution for hydrogels was changed to include anti-CD28 as well as anti-CD3 (ratio 1:1; [total biotinylated protein] = 10 μg/mL). Furthermore, the hydrogels were seeded with the same cell concentration of 1×10^6 cells/mL, as recommended for Dynabead T cell activation and expansion. Soft (0.05% w/v cross-linker) and stiff (0.4% w/v cross-linker) hydrogels were evaluated. Dynabeads were prepared according to the manufacturer's instructions and mixed with cells at a 1:1 cell-to-bead in tissue culture plates. The DynaMag-2 magnet was used to aggregate beads during washing steps and separate them from cells before sample collection. Uncoated tissue culture plastic (TCP) was used as a negative control. IL-2 secretion was assayed at 6, 24, and 48 h. At 48 h of stimulation, cells were reseeded at a concentration of 5×10^5 cells/mL in new tissue culture plates and then cultured for another 6 days. During this proliferation period, cell numbers and diameters were measured every 2 days. Fresh medium was added to the culture wells at the same time points.

2.9. Cell Spreading. For cell morphology analysis, images of cells on gels (20× magnification) were taken at 6 and 24 h of anti-CD3/CD28 stimulation using a Zeiss Primovert phase contrast microscope equipped with a 5-megapixel camera (Axiocam 105 color). Cell spreading areas were measured (total ≥60 cells from 3 gels per condition) using Fiji (version 2.0.0-rc-65/1.51w).

2.10. IL-2 ELISA. IL-2 secretion was used as a functional readout of T cell activation and measured by ELISA. All IL-2 ELISAs were performed using a commercial kit, according to the manufacturer's instructions. Briefly, the concentration of IL-2 for each sample was calculated from the optical density values measured by a Multiskan FC microplate reader (Thermo Scientific). All IL-2 standards and supernatants were assayed in duplicates,and background values (culture medium-only) were subtracted from them. To account for optical imperfections in the microwell plate, readings at 540 nm were subtracted from those at 450 nm, as per the manufacturer's instructions. Standard curves were generated with a recombinant human IL-2 standard (provided by the ELISA kit) and plotted using a third-order polynomial interpolation on GraphPad Prism 6.0.

2.11. Statistical Analyses. All statistical tests were performed using R (version 3.6.1) on RStudio (version 1.2.500). Statistical significance for all tests was set at $p < 0.05$. Levene's test and the Shapiro–Wilk test were employed to assess the homogeneity of variances and normality, respectively. For data that followed the assumption of homogeneous variances, Tukey's test was used for post-hoc analysis. For those that violated the assumption, the Games–Howell test (R package: "tadaatoolbox") was used instead. For cytokine secretion data, negative controls were excluded from statistical analyses because their inclusion would reduce the statistical power to detect differences between (treated) groups pertinent to the experimental questions.

Fluorescence characterization of ligand density and hydrogel stiffness data were analyzed using one-way analysis of variance (ANOVA) followed by Tukey's post-hoc test for pairwise comparisons of means. Hydrogel stiffness measurements violated the assumption of homogeneity of variance. Therefore, the data were analyzed with one-way ANOVA with Welch's correction followed by Games–Howell post-hoc analysis.

Jurkat cell cytokine secretion was tested in multifactorial experiments, and two-way ANOVA was employed to analyze the data. The interaction model of ANOVA was used when the interaction effect between factors was significant. Otherwise, the additive model was employed. In some cases, the main effect (defined as that of one independent variable on the dependent variable, averaged across all levels of other independent variables) was significant but not the interaction. In those situations, a post-hoc analysis was performed if the significant main effect was associated with a factor with more than 2 levels. Aligned rank transformation (ART) ANOVA (from the R package "ARTool") was utilized to analyze multifactorial data that were non-normal but did not violate the assumption of homogeneous variances. This decision was made because ART ANOVA is a nonparametric method that allows interaction effects to be examined. Interaction contrasts, or "differences of differences", were assessed in post-hoc analysis following ART ANOVA.

When applicable, $\log_{10}$ transformation was applied to normalize the data before statistical analysis. To improve post-analysis interpretability, the $\log_{10}$ data were back-transformed and presented on the original scale along with geometric means and 95% confidence intervals. If transformation was not required, data were presented on the original scale as means with standard deviations.

For cell area measurements, data distributions were compared (e.g., coated vs uncoated, or coated 7.1 kPa vs coated 50.6 kPa) using a two-sample Kolmogorov–Smirnov test, which does not assume normality or equal variances.

3. RESULTS

3.1. Hydrogel Stiffness. Varying the cross-linker concentration while keeping monomer concentration fixed (10% w/v) enabled tuning of hydrogel stiffness (Figure 4a). Increasing the cross-linker concentration from 0.05 to 0.4% (w/v) increased the stiffness by approximately 7-fold from 7.1 ± 0.4 to 50.6 ± 15.1 kPa.

https://dx.doi.org/10.1021/acsami.0c16478
ACS Appl. Mater. Interfaces 2020, 12, 47355–47367

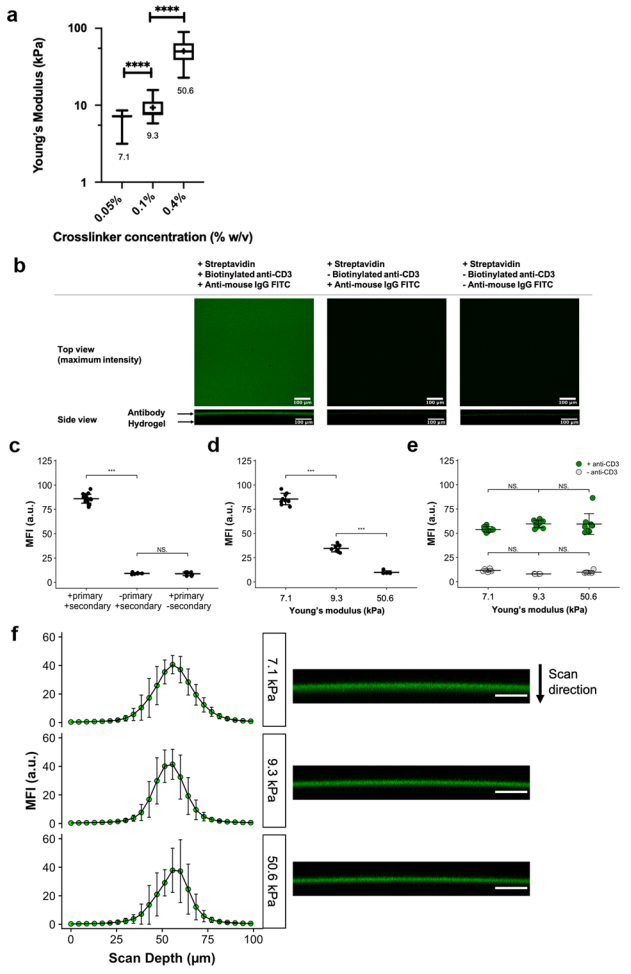

Figure 4. (a) Young's modulus of hydrogels measured via AFM-based indentation. Box-and-whisker plots: whiskers = min-max, line = median, box = 25−75%, cross (+) = mean. **** denotes $p \leq 0.0001$. Welch's ANOVA with Games−Howell post-hoc test ($\alpha = 0.05$) was used. (b) Conjugation of anti-CD3 to PA hydrogels via biotin-streptavidin capture. Top row (x−y projection): representative confocal microscopy images (top-down view) of streptavidin-doped PA hydrogels coated with biotinylated anti-CD3 and detected using FITC-conjugated anti-mouse IgG, which appears as green in the left image. Negative controls (middle and right images) showed minimal binding of the secondary antibody to the hydrogel when anti-CD3 was absent. All gels depicted here correspond to those of 7.1 kPa. Bottom row (x−z projection): representative side projections of hydrogels. The green layer visible in the left image represents the antibody layer. All scale bars are 100 μm. (c) Mean fluorescence intensities (MFIs) of hydrogels (7.1 kPa) incubated with (+) primary and secondary antibodies compared with MFIs of those without (−) either the primary or secondary. (d) Pre-normalization of surface ligand density: significant reduction in MFI was observed with increasing stiffness when the same concentration (100 μg/mL) of streptavidin-conjugated acrylamide was used. (e) Post-normalization of surface ligand density: no significant MFI differences were observed in anti-CD3-coated hydrogels. For (c−e), data = mean ± standard deviation. Data points represent individual MFI readings obtained from at least 3 separate hydrogels per condition and at least 2 ROIs per gel. *** denotes $p \leq 0.001$; NS means no significance. One-way ANOVA with Tukey's test ($\alpha = 0.05$) was used. (f) Left column: z-axis profiles of mean fluorescence intensity (MFI) versus scan depth obtained by confocal microscopy for streptavidin-doped PA hydrogels coated with biotinylated anti-CD3. Data presented as mean values with standard deviation error bars. Data points represent individual MFI readings obtained from at least 3 separate hydrogels per stiffness and at least 2 ROIs per gel. Right column: representative x−z projection images of respective hydrogels. Scale bar = 100 μm.

3.2. Surface Ligand Density Characterization.

Biotinylated anti-CD3 was successfully conjugated to streptavidin-doped PA hydrogels, as demonstrated by immunofluorescence imaging (Figure 4b). Hydrogels treated with both primary and secondary antibodies exhibited significantly higher MFI than control gels (Figure 4c). Side (x−z) projections indicated that staining was confined to the top 30−35 μm layer of the hydrogel (Figure 4b,f). For visual clarity, hydrogels were also co-labeled with FITC and Alexa Fluor 568 to show the surface confinement of antibodies (Figure S3).

It was noted that when identical concentrations of streptavidin-acrylamide were used to fabricate hydrogels of different stiffnesses, there was a significant reduction in MFI with increasing cross-linker concentration (Figure 4d). Therefore, streptavidin-acrylamide concentration was modulated with hydrogel stiffness to maintain equivalent surface ligand density for all hydrogels. After this adjustment for surface ligand density, no significant difference in MFI was observed (Figure 4e). Hydrogels produced using the optimized recipe were used for subsequent T cell stimulation experiments.

3.3. Effect of Substrate Stiffness and Ligand Density on IL-2 Secretion.

The stiffest hydrogel (50.6 kPa) stimulated higher IL-2 secretion from Jurkat cells than the softest hydrogel (7.1 kPa) (Figure 5a). At the same stiffness (7.1 kPa), increasing anti-CD3 concentration in the hydrogel coating solution from 10 to 30 μg/mL led to a significant increase in IL-2 secretion. A similar increase in IL-2 secretion was observed when cells were cultured on 9.3 kPa gels. Two-way ANOVA revealed that there was a significant interaction effect ($p = 3.83 \times 10^{-4}$) between anti-CD3 concentration and cross-linker concentration.

The stiffest and softest gels in the 10 μg/mL anti-CD3 group were also chosen for a time course experiment, where the cells were incubated with the hydrogels for various durations (Figure 5b). A more rapid increase in IL-2 secretion in the first 24 h was observed for cells incubated with the 50.6 kPa gel than for cells incubated with the 7.1 kPa gel. However, no significant difference in IL-2 secretion was observed beyond 24 h for both groups.

3.4. Comparison of T Cell Activation by Hydrogels and Dynabeads.

Hydrogels and Dynabeads coated with both primary and costimulatory signals (anti-CD3/CD28) triggered IL-2 secretion from Jurkat cells (Figure 5c). Similar to the time course experiment (Figure 5b) where hydrogels presented only anti-CD3 to the cells, the stiff gel stimulated a higher level of IL-2 secretion than the soft gel in the first 24 h. Post-hoc difference-in-differences analysis supported this observation as the differential change in IL-2 over time between the stiff gel- and soft gel-stimulated groups was significant (soft-stiff | 6 h: soft-stiff | 24 h; p-value = 1.19×10^{-4}). This change was less significant when the comparison was made between 24 and 48 h (soft-stiff | 24 h: soft-stiff | 48 h; p-value = 9.6719×10^{-3}). Dynabeads induced a modest level of IL-2 secretion compared to the two hydrogel-stimulated groups. Quantification of the number of cells interacting with Dynabeads was determined using an image processing pipeline (Figures S1, S2). These data indicate that a majority of beads were underutilized, either due to aggregation or failure to make contact with the cells.

https://dx.doi.org/10.1021/acsami.0c16478
ACS Appl. Mater. Interfaces 2020, 12, 47355−47367

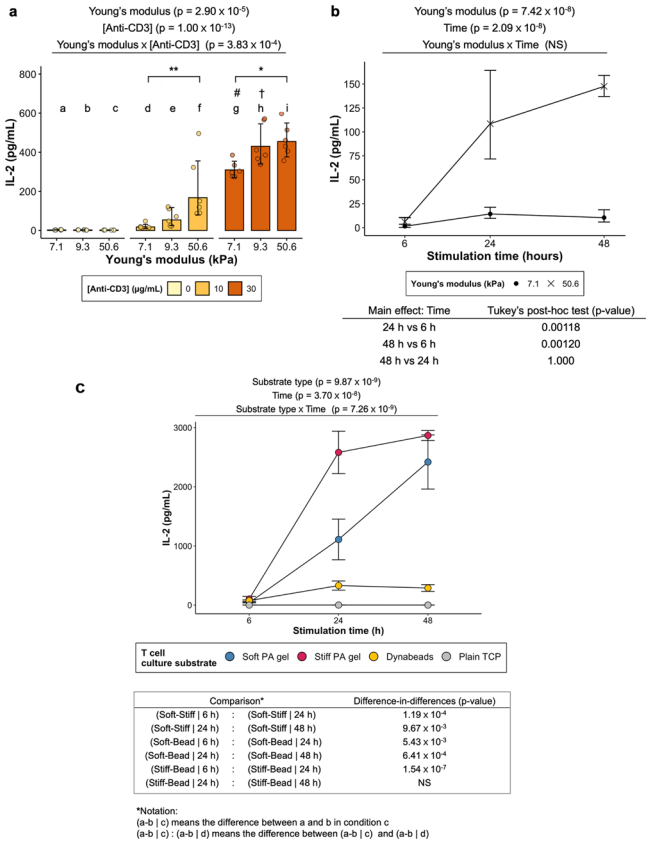

Figure 5. (a,b) Stimulation of Jurkat cells using anti-CD3-coated PA hydrogels. *P*-values returned by two-way ANOVA are noted above the plots. (a) IL-2 secretion from the cells stimulated on Ab-coated hydrogels of different formulations. *P*-values of main effects (Young's modulus and [Anti-CD3]) and interaction effect (Young's modulus × [Anti-CD3]) returned by ANOVA are noted above the plot. Data presented as geometric means with 95% confidence interval error bars back-transformed from the $\log_{10}$ scale to the original scale. Points represent individual data points from three independent experiments (N = 3). Two-way ANOVA (with interaction; White-adjusted for heteroscedasticity) on $\log_{10}$-transformed data followed by Games–Howell post-hoc test (α = 0.05). # Significant difference (p < 0.0001) from d. † Significant difference (p < 0.01) from e. * p < 0.05. ** p < 0.01. (b) The effect of stimulation time on IL-2 secretion from Jurkat cells stimulated by 7.1 (soft) and 50.6 kPa (stiff) gels. Both stiff and soft gels were coated with 10 μg/mL anti-CD3. *P*-values returned by two-way ANOVA are noted above the plots. Data presented as geometric means with 95% confidence interval error bars back-transformed from $\log_{10}$ the scale. N = 3. Two-way ANOVA on $\log_{10}$-transformed data followed by Tukey's post-hoc test on the main effect of stimulation time (α = 0.05). *P*-values from pairwise comparisons are shown below the plot. (c) IL-2 secretion by Jurkat cells stimulated by soft gels (7.1 kPa) and stiff gels (50.6 kPa) presenting both signals 1 (anti-CD3) and 2 (anti-CD28). Dynabeads presenting the same signals were included as a positive control. TCP devoid of any stimulatory signals was employed as a negative control. ART two-way ANOVA (with interaction) followed by post-hoc interaction contrast (difference-in-differences) analysis (α = 0.05). *P*-values for main effect (substrate type and time) and interaction (substrate type × time) effects returned by ANOVA are noted above the plot. Substrate type refers to the substrate material employed to stimulate Jurkat cells. Data presented as mean ± standard deviation. N = 3. Post-hoc comparisons between groups stimulated by soft gels, stiff gels, and Dynabeads are shown in the table below the plot, where the *p*-values indicate whether there is a significant difference in the differential response between a pair of substrate types for a particular stimulation time relative to that of another pair for another stimulation time. NS means not significant.

Figure 5. continued

3.5. Cell Spreading and Morphology. A significant difference (p < 0.0001) in the distribution of cell area was detected between the two anti-CD3/CD28-coated groups (50.6 vs 7.1 kPa) at both 6 and 24 h (Figure 6a,b). From 6 to 24 h, the median value for cells on 7.1 kPa (coated) increased from 132 (mean ± sd: 143 ± 58.8 μm^2) to 144 μm^2 (mean ± sd: 148 ± 26.9 μm^2), but there was a decrease from 191 (mean ± sd: 230 ± 117 μm^2) to 173 μm^2 (mean ± sd: 193 ± 66.2 μm^2) for those on 50.6 kPa (coated). Significant differences (p < 0.001 to p < 0.05) in the distribution were also observed between anti-CD3/28-coated surfaces and plain surfaces. There were markedly more outliers for 50.6 kPa than for 7.1 kPa at 6 h, indicating a greater proportion of highly spread cells on stiffer substrates. In terms of morphology, cells on the 7.1 kPa gel appeared mostly rounded (Figure 6c,d), whereas the 50.6 kPa group had noticeably more cells displaying an elongated or flattened morphology (indicated by arrows, Figure 6e,f).

3.6. Post-Stimulation Activity of Jurkat T Cells. Jurkat cells were returned to tissue culture plates after 48 h of incubation with the hydrogels or Dynabeads and monitored for a further 6 days (Figure 6g). Cells incubated with the soft hydrogels and Dynabeads proliferated more than those incubated with the stiff hydrogels. At day 4, the cell count for the stiff gel group was less than those for the other groups and the difference became more pronounced at day 6. The relatively low proliferation rate prompted further investigation into the viability of the stimulated Jurkat cells. Cell size, an established indicator of T cell metabolic fitness and activation state, was monitored using an automated cell counter.[31] Cells pre-incubated with the stiff gels had significantly smaller cell diameters on day 0 (relative to Dynabeads), day 2 (relative to all groups), and day 6 (relative to Dynabeads and soft PA gel) (Figure 6h).

4. DISCUSSION

The current study investigated the simultaneous exploitation of mechanical and biochemical cues as a potential means to regulate T cell activation. Mechanical cues were provided in the form of substrate stiffness using a PA hydrogel system. Biochemical signals were presented as antibodies against CD3 and CD28. In addition, we have created a customizable hydrogel-integrated culture device to provide insights into the effect of substrate material stiffness that will enable control of the level of stimulation. Customization was achieved by inclusion of a reversible compression-based sealing mechanism (Figure 3) that allowed for the substrate material to be changed. This obviates the need for a new device every time a different substrate material is used.

4.1. Substrate Choices and Comparisons. T cells may be stimulated using antibodies immobilized on a range of materials, such as PA hydrogels, polystyrene microbeads, TCP, or glass. These materials differ not only in stiffness but also in nano-/micro-topography, curvature, and surface chemistry, all of which could influence T cell–material interactions. Different protein conjugation strategies suitable for each material and the material's intrinsic binding capacity may also lead to

https://dx.doi.org/10.1021/acsami.0c16478
ACS Appl. Mater. Interfaces 2020, 12, 47355–47367

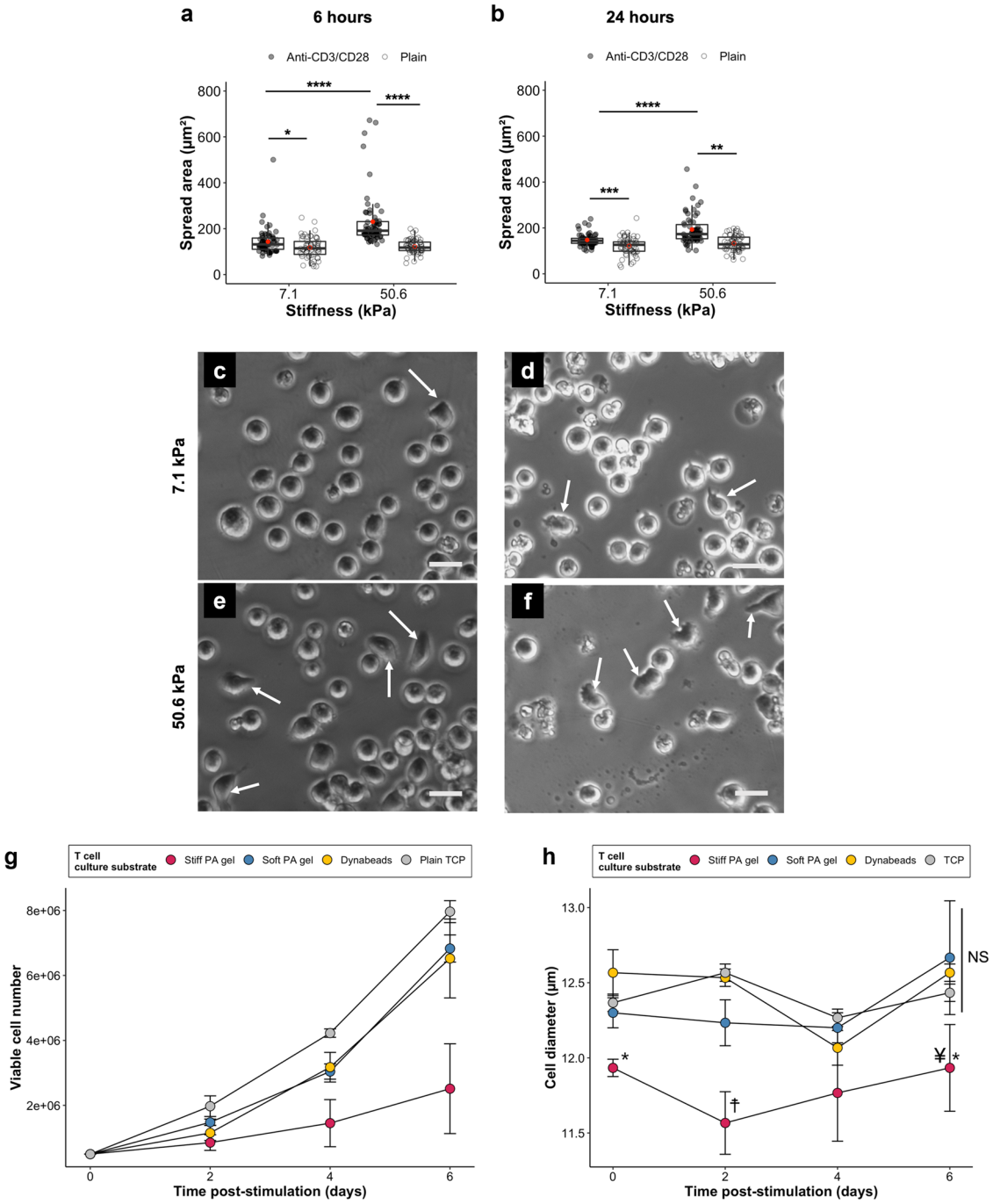

Figure 6. Spread areas of Jurkat cells after (a) 6 and (b) 24 h of stimulation on anti-CD3/CD28-coated and plain gels (7.1 vs 50.6 kPa). Measurements taken from 3 gels per condition (total ≥60 cells). Red dots represent averages. Individual data points and box-and-whisker plots are shown. *p < 0.05; **p < 0.01; ***p < 0.001; ****p < 0.0001, two-sample Kolmogorov−Smirnov test (α = 0.05). Representative phase contrast microscopy images of cells on anti-CD3/CD28-coated (c,d) 7.1 and (e,f) 50.6 kPa gels. Arrows indicate cells with a flattened or elongated morphology. Scale bars = 20 μm. (g) Post-stimulation proliferation of Jurkat cells. Data = mean ± standard deviation. N = 3. (h) Cell diameters of Jurkat cells in post-stimulation proliferation time course. Data presented as mean ± standard deviation. N = 3. Two-way ANOVA with Tukey's test (α = 0.05). * Significant difference (p < 0.01) from Dynabeads (same time). † Significant difference (p < 0.01) from all (same time). ¥ Significant difference (p < 0.001) soft PA gel (same time). NS Not significant (same time).

variations in the antibody orientation and density. Moreover, it is unlikely that T cells could deform stiff (MPa − GPa) substrates with their pico-Newton traction forces.[32] To systematically study the effect of substrate stiffness on T cell activation, we focused on PA hydrogels due to their well-known biocompatibility and mechanical tunability in the kPa range.[27] As anti-CD3/CD28 microbeads have been employed as the gold standard materials in adoptive T cell therapy trials,[33] we decided to also compare, not the stiffness-dependent effects per se, but the general stimulatory performance of our PA hydrogels against Dynabeads (Figure 5c and Figure 6g,h). Here, the comparison showed that both the stiff and soft hydrogel-stimulated groups produced more IL-2 than cells stimulated by Dynabeads dosed at the

https://dx.doi.org/10.1021/acsami.0c16478
ACS Appl. Mater. Interfaces 2020, 12, 47355−47367

manufacturer's optimized bead-to-cell ratio (Figure 5c). A possible explanation for this finding could be due to the aforementioned differences in ligand density, ligand orientation, surface chemistry, and mechanical properties between substrate types. Nevertheless, Kim Wiese et al. reported that Jurkat cells (2×10^6 cells/mL, instead of 1×10^6 cells/mL in the present study) secreted about 110 pg/mL after 24 h of stimulation by Dynabeads at a cell-to-bead ratio of 1:1.[34] In comparison, Jurkat cells in the present study secreted 76.1 ± 11.8 and 330 ± 77.7 pg/mL at 6 and 24 h, respectively (Figure 5c). Unfortunately, details regarding antibody presentation on Dynabeads are proprietary, making direct comparisons impossible.[35] Moreover, when comparing different material types, other important variables that affect T cell activation (e.g., topography and geometry) will also need to be controlled to fully decouple the influence of stiffness. Therefore, past studies have utilized Dynabeads as a positive control, not to compare the effect of stiffness, ligand density, ligand orientation, or substrate geometry, but the stimulatory performance of the custom-made biomaterials against the industry's benchmark (Dynabeads).[36,37] This kind of comparison was also employed in our study to answer the question of whether our hydrogels could produce comparable T cell activation. A second reason for using Dynabeads was for troubleshooting in case the cells did not produce the expected behavior (e.g., IL-2 secretion when cultured on anti-CD3/CD28-coated hydrogels). It should also be noted that Dynabeads are known to aggregate, which makes it difficult to estimate the true stimulatory surface area that cells are able to sense[38] (Figures S1 and S2). Furthermore, prior studies have highlighted the importance, and dominance, of the global ligand density over local ligand density, which cannot be varied much by increasing the number of beads, as they are all functionalized with the same antibody concentration.[26,39] Nevertheless, images of cell−bead contacts were taken at a single time point (48 h), and the dynamic nature of the interactions between T cells and stimulatory surfaces was not assessed.[40] Therefore, it would be useful to follow up with time-lapse imaging of immunological synapse formation as well as a titration study to determine what bead-to-cell ratio would compare with hydrogels in terms of IL-2 secretion and proliferative capacity. Results from such comparisons can then be used to assess the relative cost effectiveness of the biomaterial-based T cell stimulation strategies.

4.2. Antibody Immobilization. Using biotin-streptavidin capture, antibodies were immobilized on PA hydrogels in a robust manner, as opposed to potentially less stable physisorption methods. Although other methods (e.g., click chemistry or the SpyTag-SpyCatcher system) also allow for simple and stable antibody conjugation, they are often more costly and require additional preparation steps by the user (e.g., azido modification of the antibody and incorporation of alkyne groups into the hydrogel for click chemistry,[41] or SpyTag/SpyCatcher protein expression in *E. coli* and subsequent purification[42]). In contrast, commercially available biotin- and streptavidin-labeled reagents are more widely available and can be directly used for conjugation in their supplied format. However, a limitation was that the streptavidin concentration required optimization to normalize surface ligand density for each stiffness, as previously described[6,9] (Figure 4d e). The optimization was needed to address the diminishing ligand density with increasing stiffness, potentially due to steric and porosity-dependent effects on the accessibility of streptavidin to biotinylated antibodies.[43,44] Moreover, immobilizing antibodies in this way makes it difficult to determine the exact orientation and density of ligands presented on the surface. We therefore used antibody concentration in the coating solution as an indirect metric of ligand density, similar to how it was reported elsewhere.[45] To gain full control over the spatial positioning of ligands, electron beam lithography[46] and block copolymer micelle lithography[47] may be employed. However, the cost, time, and toxic reagents needed to produce such substrates raise the question of whether they can truly be considered an alternative to Dynabeads, which are more scalable and biocompatible.

4.3. Mechanical Characterization of PA Hydrogels. PA hydrogels are a well-established system for controlling substrate stiffness and have been widely described.[3,27] The stiffness of hydrogels can typically be measured by oscillatory rheology or AFM indentation.[48] We used AFM indentation to measure gel stiffness because, while rheological methods characterize bulk mechanical properties, AFM indentation resembles more closely how a cell would probe the fibrous network of a hydrogel. This is because T cells attach to anti-CD3-coated surfaces via transmembrane TCR-CD3 complexes. The engagement of TCR-CD3 complexes with immobilized ligands triggers cytoskeletal rearrangement, which leads to forces being exerted through TCR-CD3 complexes, providing a means for cells to mechanically deform their extracellular surroundings.[49,50] Therefore, the ideal measurement to understand how a cell senses substrate stiffness is likely to be on a cellular scale.

The measured stiffness range of ∼7 to ∼51 kPa (Figure 4a) is comparable to ranges previously reported to influence T cell activation.[6,8] Although swelling behaviors of the gels were not monitored in the current study, it has been shown that hydrogels fabricated from similar cross-linker concentrations (0.05 to 0.3% (w/v) bis-acrylamide) have low swelling ratios (between 1 and 2.1) over 71 h.[51]

4.4. Hydrogel-Integrated Culture Device for Non-Adherent Cell Culture. Fabricating 2D PA hydrogels on glass coverslips is commonly used in the field of mechanobiology, including previous studies investigating T cell activation.[6,8,27] Despite their common usage, gel-coated coverslips typically have a smaller diameter than wells of tissue culture plates. A proportion of the cells will fall into the gaps formed at the edges resulting in them interacting with TCP, rather than the stimulatory and mechanical cues provided by the hydrogel. Individually fabricated gel-coated coverslips also require increased handling and are prone to inverting or breakage. To circumvent these issues, gels may be directly polymerized inside the wells of a glass-bottom multiwell plate, but that would require additional chemical modifications to the plate and multiple manual steps to create custom gel-casting equipment.[52] Commercially available PA hydrogel-coated multiwell plates do exist, such as Matrigen's Softwell products and Ibidi μ-angiogenesis slides. However, these plates are costly, single-use, and difficult to mechanically characterize in the format supplied. Additionally, only a limited number of elasticities (three) are available for the Ibidi μ-angiogenesis slides, and coatings (collagen and fibronectin) are more suitable for adherent cell culture than T cell stimulation. The material chemistry of their surfaces is not stated, and so, it would be difficult to determine the suitable conjugation approach for antibody immobilization. Furthermore, the elastic substrate does not entirely cover the well bottom. Although the

https://dx.doi.org/10.1021/acsami.0c16478
ACS Appl. Mater. Interfaces 2020, 12, 47355−47367

Ibidi μ-angiogenesis slides are compatible with collagen, Matrigel, and agarose gels, there is no information on how PA hydrogels can be polymerized in (or attached to) the wells. Addressing these challenges, we created a multiwell device with a replaceable hydrogel substrate for the culture of cells (Figure 3). The device may be manufactured in an automated manner using common manufacturing technologies (such as micromilling or 3D printing) and so can be easily reproduced or modified by academic laboratories. Moreover, the device's microwell format can reduce the costs of experiments by permitting the use of low volumes and multiple studies to be run on a single hydrogel.

In terms of cell−material interaction in the device, it was observed that at 6−24 h post-seeding, most of the cells settled at the bottom of the wells without substantially overlapping and thereby made contact with antibody-coated surfaces (Figure 6c−f). However, the number of cells in contact with the stimulatory surface would have likely changed as a function of time as adjacent cells changed in size (Figure 6a,b) or morphology (Figure 6c−f). These changes can take place within minutes of contact with the stimulatory substrate[25,49] and hence prompt for time-lapse images to be taken.

Nevertheless, further improvements can be made to the device − namely, adopting a chimney well design to further minimize contamination risks and including a lid with condensation rings similar to that of standard multiwell plates (rather than a humidified Petri dish) to minimize evaporation. Furthermore, the current compression design relies on bolts that hold the top and bottom plates together. Therefore, care must be taken that there is enough pressure to maintain a leak-free seal, but not too much that it could cause damage to the glass slide within the device. Alternative approaches, such as Micronit's "load n' seal" mechanism, used in their organ-on-chip fluidic interface (Fluidic Connect PRO OOC), may be exploited to remove user dependence on sealing. This would also standardize the compression force and allow for further investigations into the effect of compression around culture wells on gel stiffness within the wells.

4.5. Relationship between Substrate Stiffness and T Cell Activation. Forces exerted on agonist TCR-ligand bonds can prolong the bond lifetime up to a certain magnitude ("catch bonds") before any further increase in force reduces the lifetime ("slip bonds").[53] In contrast, antagonist TCR-ligand bonds behave as slip bonds only. This catch-slip bond property has been proposed as one that is exploited by T cells and B cells to discriminate antigen affinities.[8,54] The role that substrate stiffness plays is that it can modulate TCR-ligand avidity by influencing the dynamic force accumulation in a TCR-ligand bond and, in turn, downstream signaling.[53] Indeed, the elevated IL-2 secretion with increasing stiffness (Figure 5a,b) could be attributed to the aforementioned catch bond effect. Stiffness may, therefore, act as a cue that helps T cells discriminate between normal and pathological environments − such as cancerous tissues[55] − which are generally associated with an increase in matrix stiffness.[56,57] Inspired by mechanical differences between normal and pathological tissues, our PA hydrogels were engineered to possess Young's moduli (Figure 4a) covering the range of normal and pathological human lymphoid organs, such as axillary lymph nodes. For example, using shear wave ultrasound, Bhatia et al. reported a significant difference between malignant (6.9−278.9 kPa) and normal (8.9−30.2 kPa) with a cutoff at 30.2 kPa (100% specificity, 61.8% accuracy).[58] A similar cutoff value was reported by Bae et al., at 30.6 kPa (90.9% specificity, 85.1% accuracy).[59] While Judokusumo et al.[6] reported a monotonic increase of IL-2 secretion with substrate stiffness, with the response plateauing between 100 and 200 kPa, our study revealed a lower stiffness threshold before reaching a plateau (no significant difference between 9.3 and 50.6 kPa) for both ligand densities tested (Figure 5a). This lower range could be due to differences in cell type and ligand density between the two studies.

While IL-2 secretion is considered a reliable marker of T cell activation,[60] the expression of cell surface markers may be monitored in future studies to further validate our findings − for example, CD69, CD25, and CD71.[61] Furthermore, there is mounting evidence that links the phenotype of T cells to their proliferative potential and antitumor toxicity.[62] Therefore, it would be of clinical relevance to study the differentiation status of activated T cells, which warrants the use of primary cells. Nevertheless, the measurement of IL-2 secretion in this proof-of-concept study provides a useful comparison as previous studies on T cell mechanobiology also adopted it as a marker of cell activation.[6,7,26] Thus, Jurkat cells were chosen precisely due to their reproducible secretion of IL-2 upon stimulation.[30]

4.6. Cell Spreading. T cells are known to spread on surfaces presenting stimulatory cues (anti-CD3/CD28),[25,49,50] which is in line with the results of our morphology study (Figure 6a−f). Changes in cell morphology upon TCR-ligand-mediated stimulation have been linked to actin polymerization, depolymerization, and retrograde flows, which contribute to traction forces exerted by T cells, via TCR-CD3 complexes.[25,49,50] In the present study, the average cell spreading area was higher on stiff (50.6 kPa) than on soft (7.1 kPa) substrates (Figure 6a,b). This trend is largely consistent with previous studies that employed PA hydrogels of similar stiffness ranges,[6,8,49] although there could be a biphasic response over a wider range.[25] Moreover, the distribution of cell area for Jurkat cells on anti-CD3/CD28 surfaces was highly skewed, with a larger spread for 50.6 kPa relative to 7.1 kPa. This result was likely due to both stiffness and contact time with the substrate as different stiffnesses could induce different proportions of cells to spread, and morphological changes are highly dynamic (spreading can take place within several minutes of contact formation).[25,49,50]

Spreading of T cells on stiff substrates has been linked to enhanced traction forces and signaling. For instance, Hu et al. reported that, while stiff substrates can induce a rapid increase and decline in signaling intermediates, the enhanced cell-edge dynamics of cells may be relevant to the lower, sustained signaling observed on soft substrates.[49] This could be a contributing factor underlying the higher IL-2 secretion on stiff gels and the slower buildup of IL-2 for the soft group (Figure 5c). Taken together, future studies would therefore benefit from continuous time-lapse imaging of the cells and their actin cytoskeleton, as well as an investigation into early TCR signaling, such as phosphorylation of the linker for activation of T cells, or zeta-chain-associated protein kinase 70.

4.7. Synergistic Effect of Substrate Stiffness and Ligand Density on T Cell Activation. It is well known that stiffness and ligand density can interact in complex ways to regulate a range of cell behaviors.[63] However, existing reports on the physical modulation of T cell activation have so far consisted of studies where either stiffness or ligand density was kept constant.[6,8,26,45] To the best of our knowledge, there is only one published study that has employed a 2D hydrogel

https://dx.doi.org/10.1021/acsami.0c16478
ACS Appl. Mater. Interfaces 2020, 12, 47355−47367

platform to investigate the effect of ligand density on T cell activation (measured in terms of $CD8^+$ T cell fold expansion).[45] Even so, stiffness- and ligand density-dependent effects in their study were still examined separately. As a proof of principle, we used the hydrogel-integrated culture device to demonstrate that ligand density and substrate stiffness synergistically potentiate T cell activation (Figure 5a). Thus, these two variables are tightly coupled and should be simultaneously considered in the design of T cell stimulatory substrates.

4.8. Substrate Stiffness as a Potential Cue to Prevent Exhaustion. It is well known that care should be taken when stimulating T cells to avoid exhaustion,[64] which could lead to upregulation of co-inhibitory molecules (e.g., PD-1), as well as a reduction in proliferative capacity and tumor killing ability. Current biomaterial-assisted strategies have focused on biochemical means to prevent or circumvent the issue, such as local delivery of PD-1-blocking antibodies[65] or CD2-induced co-stimulation.[66] In the current study, cells incubated with the stiff gel, which secreted the most IL-2, proliferated the least. This result indicates that, in addition to biochemical means, substrate stiffness may be an alternative way to modulate the balance between stimulation strength and proliferative capacity. Our data suggest that there is compromise between IL-2 secretion and post-stimulation proliferation at stiffness values greater than ∼9 kPa. Further studies involving stiffness values ≥9 kPa and exceeding 50 kPa are required to establish the upper limit so that the stiffness range of biomaterials may be mechanically optimized to avoid any detrimental effects on post-stimulation proliferation.

Additionally, the mechanical memory of various cell types (e.g., mesenchymal stem cells[67] and epithelial cells[68]) in the context of substrate stiffness has been described. Coupled with recent findings that the proliferative capacity of exhausted T cells can be rescued using soft stimulatory materials,[36] it would be interesting to also investigate the impact of transferring T cells from stiff to soft stimulatory substrates (and vice versa), in terms of cell differentiation and proliferation.

The accompanying smaller cell diameter observed in the stiff gel group during the proliferation period further supports this (Figure 6h). Further phenotypic analysis would be needed to dissect the exact nature of the observed cellular dysfunction.[69] It should also be noted that while the current model system (Jurkat T cell line) recapitulates many aspects of TCR signaling, primary human T cells may respond differently to the same stimuli.[30] Moreover, inter-donor variability will need to be evaluated to establish the potential utility of the current approach in a clinical setting.

For use in bioprocessing immunotherapy products, it would be counterproductive to activate T cells in a way that hinders their subsequent proliferative capacity and in vivo persistence. Attention should be given to fine-tuning the stiffness and ligand density of the substrate to enable better control of T cell activation. In this case, the softer (7.1 kPa) hydrogel may be better suited as an immunostimulatory material than the stiffer (50.6 kPa) hydrogel.

5. CONCLUSIONS

In this work, antibody-coated PA hydrogels were integrated with a customizable multiwell culture device to demonstrate the dependence of T cell activation on substrate stiffness and ligand density. Unlike the conventional method of using gel-coated coverslips, the culture device provided surfaces fully covered by a stimulatory hydrogel for T cell stimulation. We used the device to reveal that the synergistic interaction between stiffness and ligand density can be harnessed to potentiate activation. Furthermore, we showed that, in addition to common biochemical means, stiffness may be a potential mechanical approach that can be exploited to prevent cellular dysfunctions, such as exhaustion. Based on these findings, the soft hydrogel formulated would be more favorable than the stiff hydrogel in cell processing as the former stimulated higher IL-2 secretion and has a comparable proliferation rate to Dynabeads. The insights from the present study should benefit from further phenotypic analyses to elucidate how the different cue combinations can affect differentiation in the context of primary human T cells as differentiation status is known to have a significant impact on the efficacy of adoptive immunotherapy.[70]

■ ASSOCIATED CONTENT

Supporting Information

The Supporting Information is available free of charge at https://pubs.acs.org/doi/10.1021/acsami.0c16478.

Method for image processing, results for image-based cell/bead detection, MATLAB code used for cell/bead detection, fluorescence images of antibody-coated hydrogel, and T cell viabilities after 48 h of stimulation (PDF)

■ AUTHOR INFORMATION

Corresponding Author

Richard M. Day − *Centre for Precision Healthcare, Division of Medicine and Centre for Nature Inspired Engineering, University College London, London WC1E 6BT, United Kingdom;* orcid.org/0000-0002-3124-2294; Email: r.m.day@ucl.ac.uk

Authors

Matthew H. W. Chin − *Centre for Precision Healthcare, Division of Medicine and Centre for Nature Inspired Engineering, University College London, London WC1E 6BT, United Kingdom*

Michael D. A. Norman − *Centre for Craniofacial and Regenerative Biology, King's College London, London SE1 9RT, United Kingdom*

Eileen Gentleman − *Centre for Craniofacial and Regenerative Biology, King's College London, London SE1 9RT, United Kingdom*

Marc-Olivier Coppens − *Centre for Nature Inspired Engineering and Department of Chemical Engineering, University College London, London WC1E 6BT, United Kingdom;* orcid.org/0000-0002-1810-2537

Complete contact information is available at: https://pubs.acs.org/10.1021/acsami.0c16478

Notes

The authors declare no competing financial interest.

■ ACKNOWLEDGMENTS

This work was supported by the Biotechnology and Biological Sciences Research Council (BBSRC) [grant number BB/M009513/1], the Engineering and Physical Sciences Research Council (EPSRC) "Frontier Engineering: Progression" Award [grant number EP/S03305X/1] and UCL Grand Challenges

Doctoral Students' Small Grants Scheme. Figure 1, was created with BioRender.com.

REFERENCES

(1) Ingber, D. E.; Folkman, J. Mechanochemical Switching between Growth and Differentiation during Fibroblast Growth Factor-Stimulated Angiogenesis in Vitro: Role of Extracellular Matrix. *J. Cell Biol.* **1989**, *109*, 317−330.

(2) Pirone, D. M.; Liu, W. F.; Ruiz, S. A.; Gao, L.; Raghavan, S.; Lemmon, C. A.; Romer, L. H.; Chen, C. S. An Inhibitory Role for FAK in Regulating Proliferation: A Link between Limited Adhesion and RhoA-ROCK Signaling. *J. Cell Biol.* **2006**, *174*, 277−288.

(3) Engler, A. J.; Sen, S.; Sweeney, H. L.; Discher, D. E. Matrix Elasticity Directs Stem Cell Lineage Specification. *Cell* **2006**, *126*, 677−689.

(4) Huang, S.; Ingber, D. E. Cell Tension, Matrix Mechanics, and Cancer Development. *Cancer Cell* **2005**, *8*, 175−176.

(5) Discher, D. E.; Janmey, P.; Wang, Y.-L. Tissue Cells Feel and Respond to the Stiffness of Their Substrate. *Science* **2005**, *310*, 1139−1143.

(6) Judokusumo, E.; Tabdanov, E.; Kumari, S.; Dustin, M. L.; Kam, L. C. Mechanosensing in T Lymphocyte Activation. *Biophys. J.* **2012**, *102*, L5−L7.

(7) O'Connor, R. S.; Hao, X.; Shen, K.; Bashour, K.; Akimova, T.; Hancock, W. W.; Kam, L. C.; Milone, M. C. Substrate Rigidity Regulates Human T Cell Activation and Proliferation. *J. Immunol.* **2012**, *189*, 1330−1339.

(8) Saitakis, M.; Dogniaux, S.; Goudot, C.; Bufi, N.; Asnacios, S.; Maurin, M.; Randriamampita, C.; Asnacios, A.; Hivroz, C. Different TCR-Induced T Lymphocyte Responses Are Potentiated by Stiffness with Variable Sensitivity. *Elife* **2017**, *6*, No. e23190.

(9) Wan, Z.; Zhang, S.; Fan, Y.; Liu, K.; Du, F.; Davey, A. M.; Zhang, H.; Han, W.; Xiong, C.; Liu, W. B Cell Activation Is Regulated by the Stiffness Properties of the Substrate Presenting the Antigens. *J. Immunol.* **2013**, *190*, 4661−4675.

(10) Basu, R.; Whitlock, B. M.; Husson, J.; Le Floc'h, A.; Jin, W.; Oyler-Yaniv, A.; Dotiwala, F.; Giannone, G.; Hivroz, C.; Biais, N.; Lieberman, J.; Kam, L. C.; Huse, M. Cytotoxic T Cells Use Mechanical Force to Potentiate Target Cell Killing. *Cell* **2016**, *165*, 100−110.

(11) June, C. H. Principles of Adoptive T Cell Cancer Therapy. *J Clin Invest* **2007**, *117*, 1204−1212.

(12) Grupp, S. A.; Kalos, M.; Barrett, D.; Aplenc, R.; Porter, D. L.; Rheingold, S. R.; Teachey, D. T.; Chew, A.; Hauck, B.; Wright, J. F.; Milone, M. C.; Levine, B. L.; June, C. H. Chimeric Antigen Receptor-Modified T Cells for Acute Lymphoid Leukemia. *N. Engl. J. Med.* **2013**, *368*, 1509−1518.

(13) Lu, Y.-C.; Parker, L. L.; Lu, T.; Zheng, Z.; Toomey, M. A.; White, D. E.; Yao, X.; Li, Y. F.; Robbins, P. F.; Feldman, S. A.; Van Der Bruggen, P.; Klebanoff, C. A.; Goff, S. L.; Sherry, R. M.; Kammula, U. S.; Yang, J. C.; Rosenberg, S. A. Treatment of Patients with Metastatic Cancer Using a Major Histocompatibility Complex Class II-Restricted T-Cell Receptor Targeting the Cancer Germline Antigen MAGE-A3. *J. Clin. Oncol.* **2017**, *35*, 3322−3329.

(14) Dudley, M. E.; Gross, C. A.; Langhan, M. M.; Garcia, M. R.; Sherry, R. M.; Yang, J. C.; Phan, G. Q.; Kammula, U. S.; Hughes, M. S.; Citrin, D. E.; Restifo, N. P.; Wunderlich, J. R.; Prieto, P. A.; Hong, J. J.; Langan, R. C.; Zlott, D. A.; Morton, K. E.; White, D. E.; Laurencot, C. M.; Rosenberg, S. A. CD8+ Enriched "Young" Tumor Infiltrating Lymphocytes Can Mediate Regression of Metastatic Melanoma. *Clin. Cancer Res.* **2010**, *16*, 6122−6131.

(15) Maude, S. L.; Laetsch, T. W.; Buechner, J.; Rives, S.; Boyer, M.; Bittencourt, H.; Bader, P.; Verneris, M. R.; Stefanski, H. E.; Myers, G. D.; Qayed, M.; De Moerloose, B.; Hiramatsu, H.; Schlis, K.; Davis, K. L.; Martin, P. L.; Nemecek, E. R.; Yanik, G. A.; Peters, C.; Baruchel, A.; Boissel, N.; Mechinaud, F.; Balduzzi, A.; Krueger, J.; June, C. H.; Levine, B. L.; Wood, P.; Taran, T.; Leung, M.; Mueller, K. T.; Zhang, Y.; Sen, K.; Lebwohl, D.; Pulsipher, M. A.; Grupp, S. A. Tisagenlecleucel in Children and Young Adults with B-Cell Lymphoblastic Leukemia. *N. Engl. J. Med.* **2018**, *378*, 439−448.

(16) Ni, K.; O'Neill, H. C. The Role of Dendritic Cells in T Cell Activation. *Immunol. Cell Biol.* **1997**, *75*, 223−230.

(17) Kershaw, M. H.; Westwood, J. A.; Darcy, P. K. Gene-Engineered T Cells for Cancer Therapy. *Nat. Rev. Cancer* **2013**, *13*, 525−541.

(18) Eggermont, L. J.; Paulis, L. E.; Tel, J.; Figdor, C. G. Towards Efficient Cancer Immunotherapy: Advances in Developing Artificial Antigen-Presenting Cells. *Trends Biotechnol.* **2014**, *32*, 456−465.

(19) Trickett, A.; Kwan, Y. L. T Cell Stimulation and Expansion Using Anti-CD3/CD28 Beads. *J. Immunol. Methods* **2003**, *275*, 251−255.

(20) Brandrup, J.; Immergut, E. H.; Grulke, E. A. *Polymer Handbook*; 2 Volumes Set, 4th Edition; JOHN WILEY & SONS INC: 2003.

(21) Li, Y.; Kurlander, R. J. Comparison of Anti-CD3 and Anti-CD28-Coated Beads with Soluble Anti-CD3 for Expanding Human T Cells: Differing Impact on CD8 T Cell Phenotype and Responsiveness to Restimulation. *J. Transl. Med.* **2010**, *8*, 104.

(22) Harrison, D. L.; Fang, Y.; Huang, J. T-Cell Mechanobiology: Force Sensation, Potentiation, and Translation. *Front. Phys.* **2019**, *7*, 45.

(23) Feng, Y.; Brazin, K. N.; Kobayashi, E.; Mallis, R. J.; Reinherz, E. L.; Lang, M. J. Mechanosensing Drives Acuity of Aβ T-Cell Recognition. *Proc. Natl. Acad. Sci. U. S. A.* **2017**, *114*, E8204−E8213.

(24) Basu, R.; Huse, M. Mechanical Communication at the Immunological Synapse. *Trends Cell Biol.* **2017**, *27*, 241−254.

(25) Wahl, A.; Dinet, C.; Dillard, P.; Nassereddine, A.; Puech, P.-H.; Limozin, L.; Sengupta, K. Biphasic Mechanosensitivity of T Cell Receptor-Mediated Spreading of Lymphocytes. *Proc. Natl. Acad. Sci. U. S. A.* **2019**, *116*, 5908−5913.

(26) Deeg, J.; Axmann, M.; Matic, J.; Liapis, A.; Depoil, D.; Afrose, J.; Curado, S.; Dustin, M. L.; Spatz, J. P. T Cell Activation Is Determined by the Number of Presented Antigens. *Nano Lett.* **2013**, *13*, 5619−5626.

(27) Tse, J. R.; Engler, A. J. Preparation of Hydrogel Substrates with Tunable Mechanical Properties. *Curr. Protoc. Cell Biol.* **2010**, 10.16.1.

(28) Körstgens, V.; Pröller, S.; Buchmann, T.; Moseguí González, D.; Song, L.; Yao, Y.; Wang, W.; Werhahn, J.; Santoro, G.; Roth, S. V.; Iglev, H.; Kienberger, R.; Müller-Buschbaum, P. Laser-Ablated Titania Nanoparticles for Aqueous Processed Hybrid Solar Cells. *Nanoscale* **2015**, *7*, 2900−2904.

(29) Hutter, J. L.; Bechhoefer, J. Calibration of Atomic-Force Microscope Tips. *Rev. Sci. Instrum.* **1993**, *64*, 1868−1873.

(30) Abraham, R. T.; Weiss, A. Jurkat T Cells and Development of the T-Cell Receptor Signalling Paradigm. *Nat. Rev. Immunol.* **2004**, *4*, 301−308.

(31) Levine, B. L.; Bernstein, W. B.; Connors, M.; Craighead, N.; Lindsten, T.; Thompson, C. B.; June, C. H. Effects of CD28 Costimulation on Long-Term Proliferation of CD4+ T Cells in the Absence of Exogenous Feeder Cells. *J. Immunol.* **1997**, *159*, 5921−5930.

(32) Liu, Y.; Blanchfield, L.; Ma, V. P.-Y.; Andargachew, R.; Galior, K.; Liu, Z.; Evavold, B.; Salaita, K. DNA-Based Nanoparticle Tension Sensors Reveal That T-Cell Receptors Transmit Defined PN Forces to Their Antigens for Enhanced Fidelity. *Proc. Natl. Acad. Sci. U. S. A.* **2016**, *113*, 5610−5615.

(33) Wang, X.; Rivière, I. Clinical Manufacturing of CAR T Cells: Foundation of a Promising Therapy. *Mol Ther Oncolytics* **2016**, *3*, 16015.

(34) Kim Wiese, A.; Schluterman Burdine, M.; Turnage, R. H.; Tackett, A. J.; Burdine, L. J. DNA-PKcs Controls Calcineurin Mediated IL-2 Production in T Lymphocytes. *PLoS One* **2017**, *12*, No. e0181608.

(35) Lambert, L. H.; Goebrecht, G. K. E.; De Leo, S. E.; O'Connor, R. S.; Nunez-Cruz, S.; Li, T.-D.; Yuan, J.; Milone, M. C.; Kam, L. C. Improving T Cell Expansion with a Soft Touch. *Nano Lett.* **2017**, *17*, 821−826.

https://dx.doi.org/10.1021/acsami.0c16478
ACS Appl. Mater. Interfaces 2020, 12, 47355−47367

(36) Dang, A. P.; De Leo, S.; Bogdanowicz, D. R.; Yuan, D. J.; Fernandes, S. M.; Brown, J. R.; Lu, H. H.; Kam, L. C. Enhanced Activation and Expansion of T Cells Using Mechanically Soft Elastomer Fibers. *Adv. Biosyst.* **2018**, *2*, 1700167.
(37) Cheung, A. S.; Zhang, D. K. Y.; Koshy, S. T.; Mooney, D. J. Scaffolds That Mimic Antigen-Presenting Cells Enable Ex Vivo Expansion of Primary T Cells. *Nat. Biotechnol.* **2018**, *36*, 160−169.
(38) Piscopo, N. J.; Mueller, K. P.; Das, A.; Hematti, P.; Murphy, W. L.; Palecek, S. P.; Capitini, C. M.; Saha, K. Bioengineering Solutions for Manufacturing Challenges in CAR T Cells. *Biotechnol. J.* **2018**, *13*, 1700095.
(39) Majedi, F. S.; Hasani-Sadrabadi, M. M.; Thauland, T. J.; Li, S.; Bouchard, L.-S.; Butte, M. J. Augmentation of T-Cell Activation by Oscillatory Forces and Engineered Antigen-Presenting Cells. *Nano Lett.* **2019**, 6945.
(40) Gunzer, M.; Schäfer, A.; Borgmann, S.; Grabbe, S.; Zänker, K. S.; Bröcker, E. B.; Kämpgen, E.; Friedl, P. Antigen Presentation in Extracellular Matrix: Interactions of T Cells with Dendritic Cells Are Dynamic, Short Lived, and Sequential. *Immunity* **2000**, *13*, 323−332.
(41) Kahveci, M. U.; Ciftci, M.; Evran, S.; Timur, S.; Yagci, Y. Photoinduced in Situ Formation of Clickable PEG Hydrogels and Their Antibody Conjugation. *Des. Monomers Polym.* **2015**, *18*, 129−136.
(42) Zakeri, B.; Fierer, J. O.; Celik, E.; Chittock, E. C.; Schwarz-Linek, U.; Moy, V. T.; Howarth, M. Peptide Tag Forming a Rapid Covalent Bond to a Protein, through Engineering a Bacterial Adhesin. *Proc. Natl. Acad. Sci. U. S. A.* **2012**, *109*, E690−E697.
(43) Lin, S.; Gu, L. Influence of Crosslink Density and Stiffness on Mechanical Properties of Type I Collagen Gel. *Materials* **2015**, *8*, 551−560.
(44) Mullen, C. A.; Vaughan, T. J.; Billiar, K. L.; McNamara, L. M. The Effect of Substrate Stiffness, Thickness, and Cross-Linking Density on Osteogenic Cell Behavior. *Biophys. J.* **2015**, *108*, 1604−1612.
(45) Hickey, J. W.; Dong, Y.; Chung, J. W.; Salathe, S. F.; Pruitt, H. C.; Li, X.; Chang, C.; Fraser, A. K.; Bessell, C. A.; Ewald, A. J.; Gerecht, S.; Mao, H.-Q.; Schneck, J. P. Engineering an Artificial T-Cell Stimulating Matrix for Immunotherapy. *Adv. Mater.* **2019**, *31*, 1807359.
(46) Cai, H.; Muller, J.; Depoil, D.; Mayya, V.; Sheetz, M. P.; Dustin, M. L.; Wind, S. J. Full Control of Ligand Positioning Reveals Spatial Thresholds for T Cell Receptor Triggering. *Nat. Nanotechnol.* **2018**, *13*, 610−617.
(47) Wang, X.; Li, S.; Yan, C.; Liu, P.; Ding, J. Fabrication of RGD Micro/Nanopattern and Corresponding Study of Stem Cell Differentiation. *Nano Lett.* **2015**, *15*, 1457−1467.
(48) Oyen, M. L. Mechanical Characterisation of Hydrogel Materials. *Int. Mater. Rev.* **2014**, *59*, 44−59.
(49) Hui, K. L.; Balagopalan, L.; Samelson, L. E.; Upadhyaya, A. Cytoskeletal Forces during Signaling Activation in Jurkat T-Cells. *Mol. Biol. Cell* **2015**, *26*, 685−695.
(50) Bashour, K. T.; Gondarenko, A.; Chen, H.; Shen, K.; Liu, X.; Huse, M.; Hone, J. C.; Kam, L. C. CD28 and CD3 Have Complementary Roles in T-Cell Traction Forces. *Proc. Natl. Acad. Sci. U. S. A.* **2014**, *111*, 2241−2246.
(51) Wu, P. J.; Kabakova, I. V.; Ruberti, J. W.; Sherwood, J. M.; Dunlop, I. E.; Paterson, C.; Török, P.; Overby, D. R. Water Content, Not Stiffness, Dominates Brillouin Spectroscopy Measurements in Hydrated Materials. *Nat. Methods* **2018**, *15*, 561−562.
(52) Mih, J. D.; Sharif, A. S.; Liu, F.; Marinkovic, A.; Symer, M. M.; Tschumperlin, D. J. A Multiwell Platform for Studying Stiffness-Dependent Cell Biology. *PLoS One* **2011**, *6*, No. e19929.
(53) Liu, B.; Chen, W.; Evavold, B. D.; Zhu, C. Accumulation of Dynamic Catch Bonds between TCR and Agonist Peptide-MHC Triggers T Cell Signaling. *Cell* **2014**, *157*, 357−368.
(54) Natkanski, E.; Lee, W. Y.; Mistry, B.; Casal, A.; Molloy, J. E.; Tolar, P. B Cells Use Mechanical Energy to Discriminate Antigen Affinities. *Science* **2013**, *340*, 1587−1590.
(55) Paszek, M. J.; Zahir, N.; Johnson, K. R.; Lakins, J. N.; Rozenberg, G. I.; Gefen, A.; Reinhart-King, C. A.; Margulies, S. S.; Dembo, M.; Boettiger, D.; Hammer, D. A.; Weaver, V. M. Tensional Homeostasis and the Malignant Phenotype. *Cancer Cell* **2005**, *8*, 241−254.
(56) Pearce, O. M. T.; Delaine-Smith, R. M.; Maniati, E.; Nichols, S.; Wang, J.; Böhm, S.; Rajeeve, V.; Ullah, D.; Chakravarty, P.; Jones, R. R.; Montfort, A.; Dowe, T.; Gribben, J.; Jones, J. L.; Kocher, H. M.; Serody, J. S.; Vincent, B. G.; Connelly, J.; Brenton, J. D.; Chelala, C.; Cutillas, P. R.; Lockley, M.; Bessant, C.; Knight, M. M.; Balkwill, F. R. Deconstruction of a Metastatic Tumor Microenvironment Reveals a Common Matrix Response in Human Cancers. *Cancer Discov.* **2018**, *8*, 304−319.
(57) Acerbi, I.; Cassereau, L.; Dean, I.; Shi, Q.; Au, A.; Park, C.; Chen, Y. Y.; Liphardt, J.; Hwang, E. S.; Weaver, V. M. Human Breast Cancer Invasion and Aggression Correlates with ECM Stiffening and Immune Cell Infiltration. *Integr. Biol.* **2015**, *7*, 1120−1134.
(58) Bhatia, K. S. S.; Cho, C. C. M.; Tong, C. S. L.; Yuen, E. H. Y.; Ahuja, A. T. Shear Wave Elasticity Imaging of Cervical Lymph Nodes. *Ultrasound Med. Biol.* **2012**, *38*, 195−201.
(59) Bae, S. J.; Park, J. T.; Park, A. Y.; Youk, J. H.; Lim, J. W.; Lee, H. W.; Lee, H. M.; Ahn, S. G.; Son, E. J.; Jeong, J. Ex Vivo Shear-Wave Elastography of Axillary Lymph Nodes to Predict Nodal Metastasis in Patients with Primary Breast Cancer. *J. Breast Cancer* **2018**, *21*, 190−196.
(60) Sojka, D. K.; Bruniquel, D.; Schwartz, R. H.; Singh, N. J. IL-2 Secretion by CD4 + T Cells In Vivo Is Rapid, Transient, and Influenced by TCR-Specific Competition. *J. Immunol.* **2004**, *172*, 6136−6143.
(61) Caruso, A.; Licenziati, S.; Corulli, M.; Canaris, A. D.; De Francesco, M. A.; Fiorentini, S.; Peroni, L.; Fallacara, F.; Dima, F.; Balsari, A.; Turano, A. Flow Cytometric Analysis of Activation Markers on Stimulated T Cells and Their Correlation with Cell Proliferation. *Cytometry* **1997**, *27*, 71−76.
(62) Blaeschke, F.; Stenger, D.; Kaeuferle, T.; Willier, S.; Lotfi, R.; Kaiser, A. D.; Assenmacher, M.; Döring, M.; Feucht, J.; Feuchtinger, T. Induction of a Central Memory and Stem Cell Memory Phenotype in Functionally Active CD4+ and CD8+ CAR T Cells Produced in an Automated Good Manufacturing Practice System for the Treatment of CD19+ Acute Lymphoblastic Leukemia. *Cancer Immunol. Immunother.* **2018**, *67*, 1053−1066.
(63) Engler, A.; Bacakova, L.; Newman, C.; Hategan, A.; Griffin, M.; Discher, D. Substrate Compliance versus Ligand Density in Cell on Gel Responses. *Biophys. J.* **2004**, *86*, 617−628.
(64) Wherry, E. J. T Cell Exhaustion. *Nat. Immunol.* **2011**, *12*, 492−499.
(65) Wang, C.; Ye, Y.; Hochu, G. M.; Sadeghifar, H.; Gu, Z. Enhanced Cancer Immunotherapy by Microneedle Patch-Assisted Delivery of Anti-PD1 Antibody. *Nano Lett.* **2016**, *16*, 2334−2340.
(66) McKinney, E. F.; Lee, J. C.; Jayne, D. R. W.; Lyons, P. A.; Smith, K. G. C. T-Cell Exhaustion, Co-Stimulation and Clinical Outcome in Autoimmunity and Infection. *Nature* **2015**, *523*, 612−616.
(67) Yang, C.; Tibbitt, M. W.; Basta, L.; Anseth, K. S. Mechanical Memory and Dosing Influence Stem Cell Fate. *Nat. Mater.* **2014**, *13*, 645−652.
(68) Nasrollahi, S.; Walter, C.; Loza, A. J.; Schimizzi, G. V.; Longmore, G. D.; Pathak, A. Past Matrix Stiffness Primes Epithelial Cells and Regulates Their Future Collective Migration through a Mechanical Memory. *Biomaterials* **2017**, *146*, 146−155.
(69) Tomkowicz, B.; Walsh, E.; Cotty, A.; Verona, R.; Sabins, N.; Kaplan, F.; Santulli-Marotto, S.; Chin, C. N.; Mooney, J.; Lingham, R. B.; Naso, M.; McCabe, T. TIM-3 Suppresses Anti-CD3/CD28-Induced TCR Activation and IL-2 Expression through the NFAT Signaling Pathway. *PLoS One* **2015**, *10*, No. e0140694.
(70) Golubovskaya, V.; Wu, L. Different Subsets of T Cells, Memory, Effector Functions, and CAR-T Immunotherapy. *Cancers* **2016**, *8*, 36.

https://dx.doi.org/10.1021/acsami.0c16478
ACS Appl. Mater. Interfaces 2020, 12, 47355−47367